

Possible two-gap behavior in noncentrosymmetric superconductor $\text{Mg}_{10}\text{Ir}_{19}\text{B}_{16}$: A penetration depth study

I. Bonalde, R. L. Ribeiro, and W. Brämer-Escamilla

Centro de Física, Instituto Venezolano de Investigaciones Científicas, Apartado 20632, Caracas 1020-A, Venezuela

G. Mu and H. H. Wen

National Laboratory for Superconductivity, Beijing National Laboratory for Condensed Matter Physics and Institute of Physics, Chinese Academy of Sciences, P.O. Box 603, Beijing 100080, People's Republic of China

(Received 12 October 2008; published 24 February 2009)

We report measurements of the magnetic penetration depth $\lambda(T)$ of $\text{Mg}_{10}\text{Ir}_{19}\text{B}_{16}$ down to 50 mK ($<0.01T_c$). We observe a sample-independent small second drop around 0.8 K and an overall low-temperature response that indicate a possible two-gap superconductivity in $\text{Mg}_{10}\text{Ir}_{19}\text{B}_{16}$. A two-isotropic-gap model can account for the present penetration depth data. However, the lack of inversion symmetry in this compound with the heavy transition element Ir may lead to a large antisymmetric spin-orbit coupling that splits the spin bands and mixes spin-singlet and spin-triplet states. A model based on the two spin-split bands, with nodeless anisotropic gaps and dominant spin-triplet components, can also explain the present results. The data rule out an isotropic spin-singlet gap structure, as suggested by specific-heat measurements.

DOI: 10.1103/PhysRevB.79.052506

PACS number(s): 74.20.Rp, 74.25.Nf, 74.70.Dd

The recent discovery of superconductivity in the noncentrosymmetric heavy-fermion CePt_3Si ($T_c=0.75$ K) (Ref. 1) has sparked a lively interest in parity-violating superconductors in which the classification of the pairing states into pure even-parity spin singlet and pure odd-parity spin triplet is not possible. The absence of inversion symmetry causes the appearance of an antisymmetric potential gradient ∇V that leads to an antisymmetric spin-orbit coupling (ASOC) $\alpha(\mathbf{k} \times \nabla V) \cdot \hat{\sigma}$. Here \mathbf{k} is the electron momentum and α a coupling constant. A strong ASOC lifts the spin degeneracy existing in parity-conserving superconducting systems by originating two bands with different spin structures and with energy gaps²

$$\Delta_{\pm}(\mathbf{k}) = \psi \pm t|\mathbf{g}(\mathbf{k})|. \quad (1)$$

Here ψ and $t|\mathbf{g}(\mathbf{k})|$ are the spin-singlet and spin-triplet components, respectively, and $\mathbf{g}(\mathbf{k})$ is a dimensionless vector [$\mathbf{g}(-\mathbf{k})=-\mathbf{g}(\mathbf{k})$] parallel to the vector $\mathbf{d}(\mathbf{k})$ of the spin-triplet order parameter. In this spin-split band model the order parameter is then an admixture of spin-singlet and spin-triplet states. In this case, when the spin-orbit band splitting E_{so} is much larger than the superconducting energy scale $k_B T_c$, the system can be essentially considered a superconductor with two gaps that open at T_c . However, depending on the relative density of states of the spin-split bands, anisotropic (with and without nodes) one-gap behaviors can be realized.

The majority of the known ambient-pressure noncentrosymmetric superconductors have $E_{so} \gg k_B T_c$ (large ASOC): CePt_3Si , $\text{Li}_2(\text{Pd}, \text{Pt})_3\text{B}$,³ Re_3W ,⁴ and $\text{Mg}_{10}\text{Ir}_{19}\text{B}_{16}$.⁵ CePt_3Si (Refs. 6 and 7) and $\text{Li}_2\text{Pt}_3\text{B}$ (Refs. 8–10) have line nodes which can be explained assuming that the gapless spin-triplet component and the band with $\Delta_{-}(\mathbf{k})$ rules.¹¹ $\text{Li}_2\text{Pd}_3\text{B}$ exhibits an anisotropic nodeless behavior interpreted as a preponderant isotropic spin-singlet channel and spin-split bands contributing almost equally.⁸

Re_3W (Refs. 12 and 13) shows a somewhat unexpected

isotropic single-gap-like response, which would imply the extreme case of a highly dominant spin-split band and a preponderant isotropic spin-state component. Similar behavior has been observed in specific-heat data of $\text{Mg}_{10}\text{Ir}_{19}\text{B}_{16}$ ($T_c=5.7$ K),^{14,15} although a two-isotropic-gap function has been proposed from tunneling data.¹⁴ The latter interpretation places $\text{Mg}_{10}\text{Ir}_{19}\text{B}_{16}$ as the first noncentrosymmetric superconductor showing explicitly a two-gap-like behavior. It would be important to determine how this behavior compares to the two-gap response observed in a conventional *s*-wave superconductor with inversion symmetry such as MgB_2 . The controversial findings in $\text{Mg}_{10}\text{Ir}_{19}\text{B}_{16}$ need to be clarified in order to get further understanding on the physics of superconductors without inversion symmetry.

Here we report on measurements of the magnetic penetration depth $\lambda(T)$ of $\text{Mg}_{10}\text{Ir}_{19}\text{B}_{16}$ down to 50 mK ($<0.01T_c$). The magnetic penetration depth is a clean direct probe of the structure of the superconducting energy gap, and can readily detected nodes, small nodeless anisotropies, and multiple gaps. The penetration depth data of $\text{Mg}_{10}\text{Ir}_{19}\text{B}_{16}$ depict a small second drop at 0.8 K that flattens out around 0.2 K, an indication of a possible two-gap behavior.

$\text{Mg}_{10}\text{Ir}_{19}\text{B}_{16}$ crystallizes in a cubic crystal structure (space group $I-43m$) with large and complex unit cells of 45 atoms. The noncentrosymmetry in this compound comes from all element sites. The samples of $\text{Mg}_{10}\text{Ir}_{19}\text{B}_{16}$ used in this work, labeled A, B, and C, come from a large piece prepared using a standard method of solid-state reaction (for details on the preparation see Ref. 15). The mother sample consists of a single phase with a small amount of impurities as indicated by x-ray diffraction patterns, shows no trace of a second superconducting phase in ac susceptibility and specific-heat measurements, and displays a sharp transition in resistivity data.¹⁵ The samples A, B, and C are of granular type and have macroscopic dimensions around $0.6 \times 0.6 \times 0.4$ mm³ and superconducting onset temperatures of 5.3, 5.5, and 5.6 K, respectively. For comparison purpose we also measured a

high-purity sample of niobium ($T_c=9.2$ K). Penetration depth measurements were performed utilizing a 13 MHz tunnel diode oscillator with a frequency resolution of 15 mHz after taking into account drift effects. The magnitude of the ac field was estimated to be around 1 mOe. The internal vacuum can of the dilution refrigerator employed to get low temperatures is surrounded by a layer of CRYOPERM 10 shield which reduced the dc field at the sample to around 1 mOe. This field is 4 orders of magnitude lower than the lower critical field $H_{c1}(0)=30$ Oe.¹⁴

A change in the measured frequency with respect to the value at the lowest temperature T_{\min} is related to the variation in the magnetic susceptibility $\chi(T)$ of the sample $f(T) - f(T_{\min}) = G[\chi(T) - \chi(T_{\min})]$. The variation in the penetration depth $\Delta\lambda(T) = \lambda(T) - \lambda(T_{\min})$ is obtained through the relationship between $\chi(T)$ and $\lambda(T)$.¹⁶ The G factor depends on the empty-coil frequency and on the sample and coil geometries, and is determined by measuring a sample of known behavior and same dimensions as the test sample. For an inhomogeneous sample the effective geometry as well as the demagnetizing factor is in some degree unknown, therefore the determination of G in the present case is not reliable. We did not attempt to improve the estimation of G by using the radius-averaged susceptibility expression for a sintered sample of independent spherical grains because the samples have strongly coupled superconducting grains (see discussion in the next paragraph). The temperature variation in λ is, in any case, highly accurate and independent of G .

The normalized variations of the penetration depth $\Delta\lambda(T)/\Delta\lambda_0$ of $\text{Mg}_{10}\text{Ir}_{19}\text{B}_{16}$ and Nb are displayed in Fig. 1(a). Here $\Delta\lambda_0$ is the total penetration depth shift of the samples. The data of $\text{Mg}_{10}\text{Ir}_{19}\text{B}_{16}$ depict a sample-dependent kink around 4 K which we attribute to the intergranular component of the susceptibility of our samples. In sample C the high-temperature (above 4 K) portion of the data indicates that the effective volume fraction of the superconducting material is larger than 90%, thus the intergranular component in this sample would account only for less than 10% of the total susceptibility. The small kink, however, broadens the superconducting transition. The intergranular susceptibility usually saturates at low temperatures.

The low-temperature $\Delta\lambda(T)/\Delta\lambda_0$ of the $\text{Mg}_{10}\text{Ir}_{19}\text{B}_{16}$ samples is shown in Fig. 1(b). The data of samples A, B, and C have been shifted up for clarity. The striking features of the data for $T < 0.2T_c$ are (a) the penetration depth is temperature dependent down to the ultralow temperature $0.04T_c$ and (b) a small second drop is observed around 0.8 K. These highly reproducible features are sample independent—as opposed to the kink observed around 4 K—and, therefore, should be intrinsic properties of the superconducting phase of $\text{Mg}_{10}\text{Ir}_{19}\text{B}_{16}$. In specific-heat measurements carried out in the mother sample it was found a residual Sommerfeld coefficient $\gamma_0 \approx 13.8$ mJ/mol K² that may indicate the presence of a nonsuperconducting phase.¹⁵ These same measurements show an upturn at low temperature that was interpreted as a Schottky anomaly. The feature observed around 0.8 K in penetration depth cannot be attributed to the existence of a nonsuperconducting phase since this type of phase does not yield anomalous behaviors or unusual features in the penetration depth or the superfluid density. Nonsuperconducting

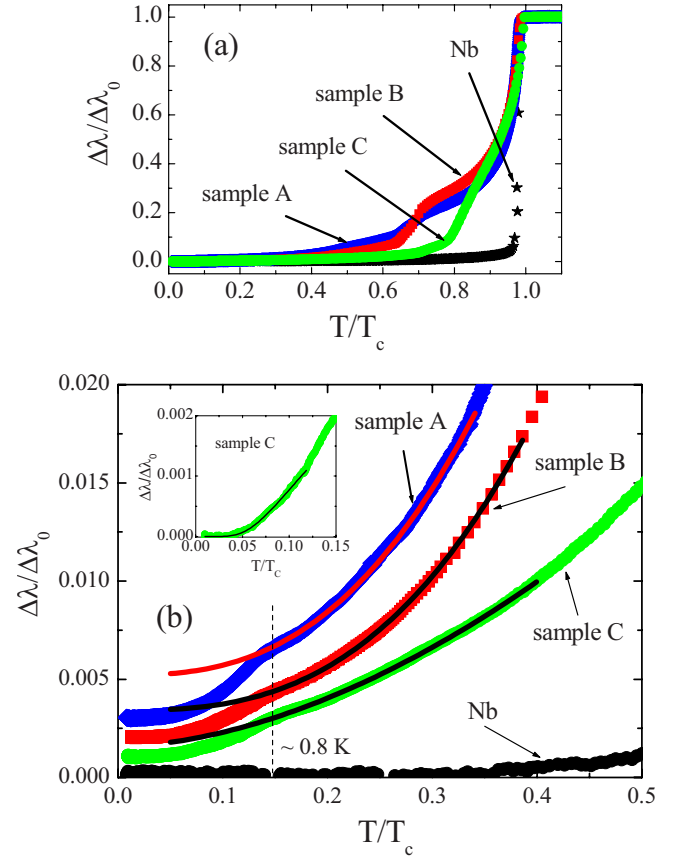


FIG. 1. (Color online) (a) Normalized temperature variation in the penetration depth for three same-batch samples of $\text{Mg}_{10}\text{Ir}_{19}\text{B}_{16}$ and for a sample of Nb. A sample-dependent kink is observed around 4 K in all samples of $\text{Mg}_{10}\text{Ir}_{19}\text{B}_{16}$. (b) Low-temperature region of the normalized temperature variation in λ . For clarity, the data of samples A, B, and C have been shifted up 0.003, 0.002, and 0.001, respectively. A clear small second drop is observed near 0.8 K in all three samples of $\text{Mg}_{10}\text{Ir}_{19}\text{B}_{16}$. The lines are fits to a power-law function (see text). The inset is a blow up of the low-temperature region showing a fit (solid line) to the BCS exponential expression at the lowest temperatures.

phases only cause an incomplete Meissner effect or shielding. Paramagnetic impurities (the type that causes the Schottky effect in specific heat) would yield an upturn, not a drop, in penetration depth (see, for example, Ref. 17).

The variation in the penetration depth at such very low temperatures is clear evidence against an isotropic s -wave energy gap, in which case the penetration depth (and any thermodynamic and transport quantity) has a BCS exponential response that flattens out below $0.2T_c$. Two previous reports on specific-heat measurements^{14,15} have provided support for an isotropic s -wave superconducting energy gap in this compound. Perhaps the low resolution and somewhat high temperatures of the specific-heat data make it difficult to resolve the small effect observed in our measurements.

In centrosymmetric superconductors a second drop in low-temperature penetration depth data would suggest the opening of a second gap. A crossover of $\lambda(T)$ from T^n ($n \approx 2$) above 0.8 K [solid lines in Fig. 1(b)] to $\{(1/\sqrt{T}) \exp[-\Delta(0)/k_B T]\}$ at the lowest measured temperatures [solid

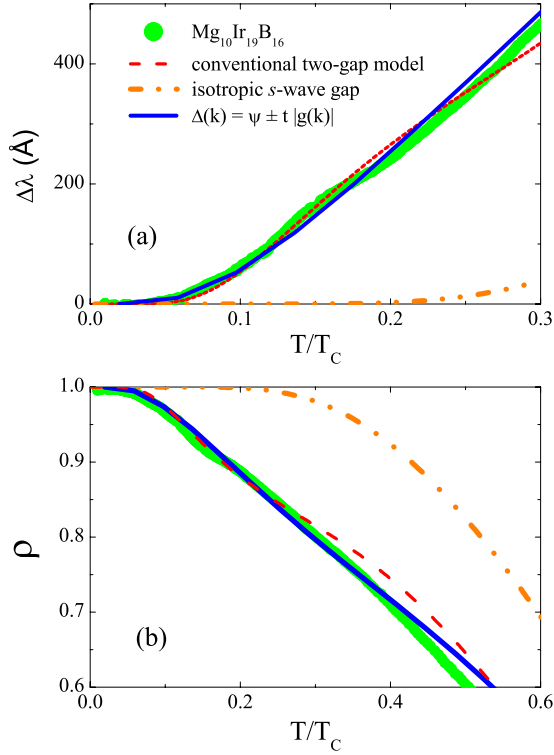


FIG. 2. (Color online) Results of the numerical evaluations of the models discussed in the text: (a) the penetration depth $\Delta\lambda(T)$ and (b) the superfluid density $[\lambda(0)/\lambda(T)]^2$. The experimental data correspond to sample C of $\text{Mg}_{10}\text{Ir}_{19}\text{B}_{16}$.

line in the inset to Fig. 1(b)] is observed in all three samples. Such a crossover from a power law to a BCS exponential behavior is expected in a conventional two-isotropic-gap system. This standard two-gap behavior would support the recent interpretation of the tunneling data of $\text{Mg}_{10}\text{Ir}_{19}\text{B}_{16}$.¹⁴ In general, the overall $\lambda(T)$ of an anisotropic single-gap superconductor would resemble that of a two-gap superconductor. However, an anisotropic single gap does not yield a marked drop in $\lambda(T)$ at low temperatures, as two gaps opening at different temperatures do and as the present penetration depth data depict at 0.8 K.

However, $\text{Mg}_{10}\text{Ir}_{19}\text{B}_{16}$ is presumably a strong noncentrosymmetric superconductor and the large spin-orbit band splitting should be considered in the analysis of the data. In the spin-split band model the gaps open at T_c and the small drop observed at low temperatures would signal some kind of anisotropy of the gaps (see below for a further discussion). An important clue on the origin of the two-gap structure would come from spin-orbit-included band-structure calculations and/or quantum oscillation measurements, neither of which has been yet reported for $\text{Mg}_{10}\text{Ir}_{19}\text{B}_{16}$.

To get further insight into the symmetry of the gap structure of $\text{Mg}_{10}\text{Ir}_{19}\text{B}_{16}$ we compare the experimental data of the magnetic penetration depth and the superfluid density with numerical evaluations of three models: (1) spin-split bands, as introduced in Eq. (1); (2) single isotropic gap (*s*-wave gap), which has been suggested for this compound from two sets of specific-heat measurements;^{14,15} and (3) two isotropic gaps (two gap), which would be valid in the hypothetical

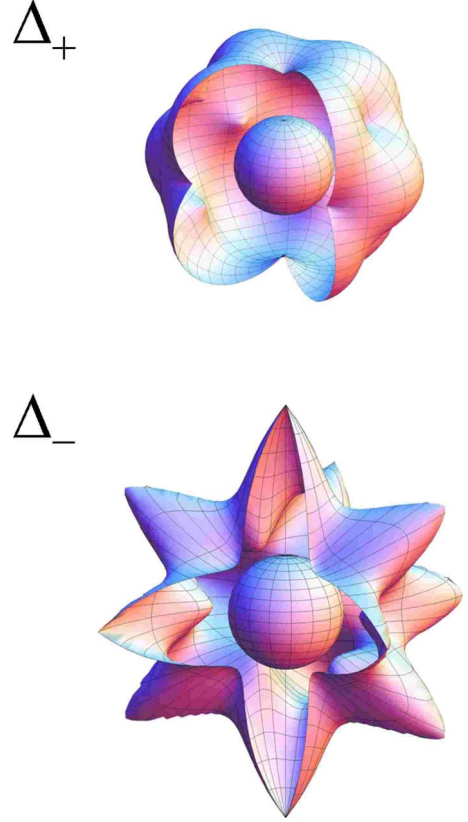


FIG. 3. (Color online) Three-dimensional (3D) polar plots of possible gap functions $\Delta_+(\mathbf{k})$ and $\Delta_-(\mathbf{k})$ of the spin-split bands in $\text{Mg}_{10}\text{Ir}_{19}\text{B}_{16}$.

case that $\text{Mg}_{10}\text{Ir}_{19}\text{B}_{16}$ has a very small ASOC that does not break the spin degeneracy of the bands.

For the numerical evaluations we apply the normalized superfluid density $\rho(T) = n_s(T)/n = \lambda^2(0)/\lambda^2(T)$, where n is the total density, in the local limit of the electrodynamics

$$\rho_{ij}(T) = 1 - 3 \left\langle \hat{k}_i \hat{k}_j \left(- \frac{\partial f}{\partial E} \right) d\epsilon \right\rangle. \quad (2)$$

Here $\langle \dots \rangle$ represents an angular average over the Fermi surface and f is the Fermi function. $\hat{\mathbf{k}} = \mathbf{k}/k_F$, with k_F the Fermi momentum. The total energy $E(\mathbf{k}) = \sqrt{\epsilon^2(\mathbf{k}) + |\Delta(T, \mathbf{k})|^2}$, where ϵ is the single-particle energy measured from the Fermi surface and $\Delta(T, \mathbf{k}) = \Delta(T)\Delta(\mathbf{k})$. We considered a spherical Fermi surface and used the standard gap interpolation formula $\Delta(T) = \Delta(0) \tanh(a\sqrt{T_c/T - 1})$, with $a = 1.38$. In all calculations we used $\Delta(0)/k_B T_c = 1.9$ (Ref. 15) and $\lambda(0) = 4040$ Å.¹⁴ The results for $\Delta\lambda(T)$ and $\rho(T)$ are presented in Figs. 2(a) and 2(b), respectively.

For the *s*-wave gap and two-gap models $\Delta(T, \mathbf{k}) = \Delta(T)$ is independent of \mathbf{k} and $\langle \hat{k}_i^2 \rangle \rightarrow 1/3$ in Eq. (2). It is evident from Fig. 2 that the experimental data do not follow at all the single isotropic gap model (dash-dotted line) suggested by specific-heat results.^{14,15} Thus, the present results of the magnetic penetration depth exclude an isotropic *s*-wave gap structure in $\text{Mg}_{10}\text{Ir}_{19}\text{B}_{16}$. For the evaluation of the two-gap model (dashed line in Fig. 2) we wrote the contributions of

bands l and s as $\rho = N\rho_l + (1-N)\rho_s$, with the normalized density of states $N=0.76$ in band l with the larger gap and the ratio of the gaps $\frac{\Delta_s}{\Delta_l}=0.21$. The low-temperature data agree reasonably well with the two-isotropic-gap model. The low-temperature superfluid density of noncentrosymmetric $\text{Mg}_{10}\text{Ir}_{19}\text{B}_{16}$ looks similar to that of the parity-conserving s -wave two-gap superconductor MgB_2 .¹⁸

For the estimation of the spin-split band model [Eq. (1)] we consider the simplest form of $\mathbf{g}(\mathbf{k})$ that is compatible with the tetrahedral point group $T_d \in \mathcal{O}_h$ (assuming a spherical Fermi surface):¹⁹ $\mathbf{g}(\mathbf{k}) = [k_x(k_z^2 - k_y^2), k_y(k_x^2 - k_z^2), k_z(k_y^2 - k_x^2)]$. This $\mathbf{g}(\mathbf{k})$ vector, an f -wave spin-triplet state, has nodes on the Fermi surface. There is no experimental evidence for an anisotropic mass tensor in $\text{Mg}_{10}\text{Ir}_{19}\text{B}_{16}$. Thus, to compute $\rho(T)$ we assume that the Fermi momenta (Fermi velocities) in the split bands are equal. Then, following the notation of Ref. 11 for comparison purpose, $\rho = (1+\delta)\rho_I + (1-\delta)\rho_{II}$. Here $\delta = (N_I - N_{II}) / (N_I + N_{II})$, with $N_{I,II}$ the density of states in the split bands I and II. In this work we choose the isotropic s -wave spin-singlet pairing ψ for simplicity. The results are shown as solid lines in Fig. 2. Overall the spin-split band model follows the low-temperature experimental data slightly better than the two-gap model. We also note that the kink or drop around 0.8 K in the experimental data is more pronounced than the ones described by the models.

The spin-split band calculation yielded $\delta=0.17$ and $\nu = \frac{\psi}{t} = 0.57$, suggesting that in $\text{Mg}_{10}\text{Ir}_{19}\text{B}_{16}$ the spin-triplet component dominates, as in CePt_3Si (Ref. 11) and $\text{Li}_3\text{Pt}_2\text{B}$.⁸ Inter-

estingly, in the latter two compounds the energy gap $\Delta_{\pm}(\mathbf{k})$ has line nodes. In $\text{Mg}_{10}\text{Ir}_{19}\text{B}_{16}$ the present penetration depth data rule out the existence of line nodes. In the other ambient-pressure noncentrosymmetric superconductors with large ASOC and nodeless gap structures, $\text{Li}_3\text{Pd}_2\text{B}$ and Re_3W , the isotropic spin-singlet component seems to be highly preponderant. Then, the present results imply that $\text{Mg}_{10}\text{Ir}_{19}\text{B}_{16}$ is the first noncentrosymmetric superconductor found to have a dominant with-node spin-triplet component but with nodeless gaps. This may have to do with the fact that the spin-split bands contribute almost equally. The possible anisotropic gap structures in the spin-split bands I and II are represented in Figs. 3(a) and 3(b), respectively.

In summary, we reported on magnetic penetration depth measurements in samples of noncentrosymmetric $\text{Mg}_{10}\text{Ir}_{19}\text{B}_{16}$. The results indicate a possible two-gap behavior that can be explained assuming either a conventional two-isotropic-gap model or anisotropic gaps in the spin-split bands that originate from a large antisymmetric spin-orbit coupling in this material. In the latter case, the spin-triplet component dominates as in CePt_3Si and $\text{Li}_3\text{Pt}_2\text{B}$. The results also discard the possibility of an isotropic s -wave spin-single pairing, as suggested by specific-heat data.

We greatly appreciate discussions with D. F. Agterberg. This work was supported by FONACIT, Venezuela, Grant No. S1-2001000693.

- ¹E. Bauer, G. Hilscher, H. Michor, C. Paul, E. W. Scheidt, A. Griбанov, Y. Seropegin, H. Noël, M. Sigrist, and P. Rogl, *Phys. Rev. Lett.* **92**, 027003 (2004).
- ²P. A. Frigeri, D. F. Agterberg, A. Koga, and M. Sigrist, *Phys. Rev. Lett.* **92**, 097001 (2004).
- ³K. Togano, P. Badica, Y. Nakamori, S. Orimo, H. Takeya, and K. Hirata, *Phys. Rev. Lett.* **93**, 247004 (2004).
- ⁴R. D. Blaugher and J. K. Hulm, *J. Phys. Chem. Solids* **19**, 134 (1961).
- ⁵T. Klimczuk, Q. Xu, E. Morosan, J. D. Thompson, H. W. Zandbergen, and R. J. Cava, *Phys. Rev. B* **74**, 220502(R) (2006).
- ⁶K. Izawa, Y. Kasahara, Y. Matsuda, K. Behnia, T. Yasuda, R. Settai, and Y. Ōnuki, *Phys. Rev. Lett.* **94**, 197002 (2005).
- ⁷I. Bonalde, W. Brämer-Escamilla, and E. Bauer, *Phys. Rev. Lett.* **94**, 207002 (2005).
- ⁸H. Q. Yuan, D. F. Agterberg, N. Hayashi, P. Badica, D. VanderVelde, K. Togano, M. Sigrist, and M. B. Salamon, *Phys. Rev. Lett.* **97**, 017006 (2006).
- ⁹H. Takeya, M. ElMassalami, S. Kasahara, and K. Hirata, *Phys. Rev. B* **76**, 104506 (2007).
- ¹⁰M. Nishiyama, Y. Inada, and G. Q. Zheng, *Phys. Rev. Lett.* **98**,

047002 (2007).

- ¹¹N. Hayashi, K. Wakabayashi, P. A. Frigeri, and M. Sigrist, *Phys. Rev. B* **73**, 024504 (2006).
- ¹²Y. L. Zuev, V. A. Kuznetsova, R. Prozorov, M. D. Vannette, M. V. Lobanov, D. K. Christen, and J. R. Thompson, *Phys. Rev. B* **76**, 132508 (2007).
- ¹³Y. Huang, J. Yan, Y. Wang, L. Shan, Q. Luo, W. Wang, and H. H. Wen, *Supercond. Sci. Technol.* **21**, 075011 (2008).
- ¹⁴T. Klimczuk, F. Ronning, V. Sidorov, R. J. Cava, and J. D. Thompson, *Phys. Rev. Lett.* **99**, 257004 (2007).
- ¹⁵G. Mu, Y. Wang, L. Shan, and H. H. Wen, *Phys. Rev. B* **76**, 064527 (2007).
- ¹⁶J. R. Thompson *et al.*, in *Magnetic Susceptibility of Superconductors and Other Spin Systems*, edited by R. A. Hein (Plenum Press, New York, 1991), p. 157.
- ¹⁷R. Prozorov, R. W. Giannetta, P. Fournier, and R. L. Greene, *Phys. Rev. Lett.* **85**, 3700 (2000).
- ¹⁸F. Manzano, A. Carrington, N. E. Hussey, S. Lee, A. Yamamoto, and S. Tajima, *Phys. Rev. Lett.* **88**, 047002 (2002).
- ¹⁹D. Agterberg (private communication).